

PAPER • OPEN ACCESS

Relating the near SOL transport with plasma properties of the confined edge region in ASDEX Upgrade

To cite this article: H J Sun *et al* 2019 *Plasma Phys. Control. Fusion* **61** 014005

View the [article online](#) for updates and enhancements.

Recent citations

- [Scrape-off layer \(SOL\) power width scaling and correlation between SOL and pedestal gradients across L, I and H-mode plasmas at ASDEX Upgrade](#)
D Silvagni *et al*
- [Scrape-off layer transport and filament characteristics in high-density tokamak regimes](#)
N. Vianello *et al*
- [Overview of physics studies on ASDEX Upgrade](#)
H. Meyer *et al*



IOP | ebooks™

Bringing you innovative digital publishing with leading voices to create your essential collection of books in STEM research.

Start exploring the collection - download the first chapter of every title for free.

Relating the near SOL transport with plasma properties of the confined edge region in ASDEX Upgrade

H J Sun¹ , E Wolfrum¹, T Eich¹ , B Kurzan¹, A Kallenbach¹ , T Happel¹, U Stroth^{1,2} and the ASDEX Upgrade Team

¹Max Planck Institute for Plasma Physics, Boltzmannstr. 2, D-85748 Garching, Germany

²Physik-Department E28, Technische Universität München, D-85747 Garching, Germany

E-mail: sunhj@ipp.mpg.de

Received 6 July 2018, revised 16 August 2018

Accepted for publication 21 September 2018

Published 12 November 2018



CrossMark

Abstract

An analysis of ASDEX Upgrade plasma is performed to understand the near SOL transport and develop the predictive basis for the electron temperature gradient, $\lambda_{T_{e,u}}$. All of the unseeded L- and H-mode attached and N seeded H-mode discharges studied are shown that the analyzed ASDEX Upgrade dataset is in the conduction-limited regime, i.e. the parallel transport in the near SOL is dominated by Spitzer–Härm conduction. By studying a H–L back transition, it is shown that the ‘bifurcation’ in the core plasma between H- and L-mode regimes also exists in the perpendicular transport in the near SOL region. Through power balance and the Spitzer–Härm conduction, the SOL perpendicular transport can be derived as $\chi_{\perp} \propto C_{H,L}^X n_e^{-1} T_e^{3/2}$, with $C_L^X / C_H^X \approx 2$. For detached plasmas, the SOL upstream electron profile is found to be broader than an equivalent attached plasma under certain conditions. By comparing $\lambda_{T_{e,u}}$ with global energy confinement, it is found that the discharges with broadened profiles also have degraded confinement, while those with unchanged profiles have similar confinement to attached plasma. The widening of the SOL is also found to coincide with the dropping of upstream temperature. Finally, comparisons of a N seeded H-mode with high pedestal top pressure and an I-mode plasma with an L-mode reference are both found to break the generally observed correlation between the T_e SOL decay length and the pedestal top pressure. Thus, the relationship is shown to be non-causal and must instead be due to similar dependences on other plasma parameters. This means that higher global energy confinement is not necessarily imply larger heat flux in the divertor and motivates the search for regimes that optimize both. The implications of these results for SOL transport are discussed.


Keywords: the SOL width, power exhaust, plasma confinement, detached condition

(Some figures may appear in colour only in the online journal)

1. Introduction

The power decay width in the scrape-off layer (SOL) [1], $\lambda_{q_{||}}$, is its most important properties since it determines the amount

of solid surface involved in plasma power exhaust which, in turn, governs the problems of target heat removal, melting, etc. SOL profiles and the power decay width are determined by a competition between transport processes perpendicular and parallel to the magnetic field. Parallel SOL transport is predicted to be classical and dominated by Spitzer–Härm conduction. This has been demonstrated to be the case experimentally for a wide range of H- and L-mode plasmas in the ASDEX Upgrade tokamak (AUG) [2–4]. For the plasma

 Original content from this work may be used under the terms of the [Creative Commons Attribution 3.0 licence](https://creativecommons.org/licenses/by/3.0/). Any further distribution of this work must maintain attribution to the author(s) and the title of the work, journal citation and DOI.

with sufficient high collisionality, filaments have been shown to enhance perpendicular transport towards the first wall which could be a concern for next step devices because of the risk of damage to the plasma facing components. For moderate collisional plasma, when convective transport is neglected, higher perpendicular thermal diffusivity, χ_{\perp} , in the SOL region is favorable because it increases the power decay length, thus decreasing the heat flux to the target. A predictive understanding of χ_{\perp} is essential for reliable modeling of heat loads for future fusion devices. To date, attempts to predict χ_{\perp} from first principle models have been of limited success. Estimates of χ_{\perp} derived from experiment can provide important physics understanding and guide the development of theory. Studies comparing theoretical models for the cross-field thermal diffusivities with SOL measurements from databases of L and H-mode plasmas from Compass-D, JET and Alcator C-Mod [5, 6], found that the theories with a $\chi_{\perp} \sim T_e^{1/2}/n_e$ scaling best described the experimental data. Here n_e and T_e are the electron density and temperature respectively. A study [4] based on both H- and L-mode data on AUG concluded that two classes of model were possible: the combined dataset can be described by a single scaling or a separate scaling for H-mode and L-mode. Assuming the single scaling for both regimes, it was found that the experimental data is best described by a cross-field thermal diffusivity of $\chi_{\perp} \propto C_{\text{HL}}^{\chi} T_e^{1/2}/n_e$, where C_{HL}^{χ} is a single coefficient. This scaling is consistent with earlier studies on Compass-D, JET and Alcator C-Mod. If a ‘bifurcation’ between these two regimes is assumed, it was found that the experimental data is best described by a cross-field thermal diffusivity of $\chi_{\perp} \propto C_{\text{H,L}}^{\chi} T_e^{3/2}/n_e$, with two different pre-multiplying coefficients for the H-mode (C_{H}^{χ}) plasma and L-mode (C_{L}^{χ}) plasma. It was not possible to determine which model was correct outside of the experimental uncertainties. In this paper, a specific experiment result will be presented to distinguish these models.

The detached plasma regime is attractive for fusion machines since erosion and melting of target surfaces are reduced. Because of this, it is proposed as one of the most promising solutions to the problem of high ITER divertor power loading. In DIII-D, the decay width of the midplane temperature and power flux profiles have been observed to increase by around 20% for detached conditions [7]. In previous studies on ASDEX Upgrade [2] under detached divertor conditions, the broadening of the near SOL T_e decay length, $\lambda_{T_{e,u}}$, was found to be roughly twice that of a similar plasma under attached conditions. The broadening of $\lambda_{T_{e,u}}$ is usually accompanied by a flattening of the density profile. Density profile flattening in the SOL region has been observed in earlier studies of L-mode plasmas, where the phenomenon has been called the L-mode high density transition (HDT) [8–10]. If the Greenwald density fraction f_{GW} is larger than a certain value, the density profile in the SOL changes, flattening its gradient and giving rise to a ‘shoulder’. In further L-mode HDT studies [11], it was found that the collisionality in the divertor plays a key role in determining the onset of this transition. The radial convective particle flux associated with the filaments is found to increase after the shoulder formation

by almost an order of magnitude [12]. In the far SOL, radial heat transport is the same before and after the shoulder formation. A physical model based on turbulent radial transport manifested by radial propagation of blobs shows that the SOL width depends on both the blob drift velocity and a blob intermittency parameter in inner limited plasma configurations [13].

Understanding the correlation between the SOL region and the confined plasma region inside the separatrix is important for optimizing the performance of a future tokamak power plant. Firstly, it is desirable to maximize the energy density at the top of the H-mode pedestal regions, since this sets the amount of fusion power in a given size machine. Secondly, it is desirable to minimize plasma-material interaction outside of the confined plasma (the SOL region), to prevent wall erosion and avoid impurities and neutrals from limiting plasma performance. A study of the enhanced D-alpha H-mode in C-Mod showed that a flattened SOL pressure profile correlates with larger heat flux widths and plasmas with high stored energy tend to have narrow heat flux widths [14]. Analysis of ASDEX Upgrade density scans in H-modes found lower confinement as the power width increases [15]. Similar trends have been reported with respect to SOL density and temperature decay lengths in ASDEX Upgrade ELMy H-modes [16]. A later study [17] on ASDEX Upgrade also showed a clear transport correlation from the steep gradient layer across the separatrix into the hot part of the SOL and indicated the importance of stiff profiles in this region. All these results suggest a close correlation between the near SOL widths and the pedestal region, in the sense that one cannot be changed alone. Higher confinement is desired in the core plasma can only be achieved at the expense of a larger heat flux in the divertor. In contrast to earlier studies of the SOL region in AUG [17, 18], recent improvements of the AUG Thomson scattering (TS) system enable the regions inside and outside separatrix to be studied separately. One good example of this is the observation that the pedestal gradients can vary by a factor of 2 while the profile in SOL remains almost unchanged [2].

The rest of this paper is organized as follows: the experimental methods are briefly introduced in section 2. In section 3, the transport study in the near SOL are presented for standard H-, L-mode and N seeded discharges under attached and detached divertor conditions. Experimental observations, for H- and L-mode plasma, of the correlation between pedestal gradients and SOL profiles are presented in section 4. In section 5, the results are summarized and physics implications are discussed.

2. Experimental methods and dataset

In ASDEX Upgrade, core and SOL electron temperature and density profiles can be obtained simultaneously for one discharge by a vertical TS system [2, 19]. The system is equipped with 4 Nd:YAG lasers at 1064 nm for core profiles and 6 lasers for the edge plasma with a spatial resolution of

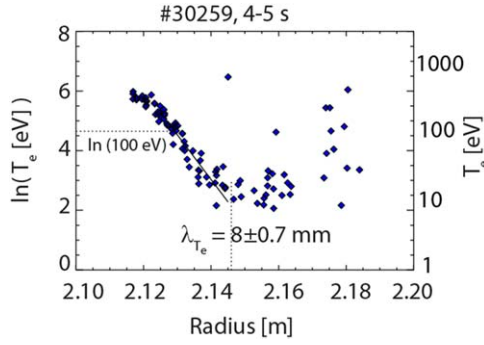


Figure 1. Log-linear plot of the electron temperature against major radius on the midplane for discharge #30259, with a fitted line (solid line) in the near SOL. The slope of the fitted line gives the decay lengths.

25 mm in the core and with a resolution of around 3 mm near the separatrix.

Based on the experimental observation that the profiles in the near SOL are exponential, consistent with all the analyzed discharges on ASDEX Upgrade, the upstream decay lengths can be evaluated by a log-linear fit in the near SOL region, a log-linear plot of a typical H-mode attached discharge can be found in figure 1. As can be seen in figure 1, the SOL profile at the midplane normally exhibit a two-layer structure. Close to the separatrix, in the so-called near SOL, the profiles have a steep exponential decay. Beyond this region, in the so-called far SOL, the profiles have an exponential decay with a much longer scale length. The temperature decay length $\lambda_{T_{e,u}}$ in this paper refer to the first, near SOL, e-folding length in the profiles, that is why they are also called midplane e-folding distance in many studies. Previous power balance analysis on ASDEX Upgrade [18] shows that the electron temperature at the separatrix is relatively insensitive to plasma parameters, and around 100 ± 20 eV. Based on this, a temperature of 100 eV ($\ln 100 \approx 4.6$) is used to determine the separatrix position. The outer most point used for fitting is that at which the far SOL starts and error bars become comparable to the measured T_e . The solid line fit to the log plot of the near SOL data gives the gradient decay lengths. The exponential nature of the profiles in the near SOL means that the measured decay length does not vary across the near SOL and so the analysis is relatively insensitive to the chosen electron temperature at the separatrix. The type I ELMy H-mode attached discharges (36 in total) and L-mode attached discharges (27 in total) used in the present dataset are the same discharges as those used in [4]. To increase the range of the plasma parameters for the parametric dependence study, nitrogen seeded discharges, which were used for the separatrix density study in [20], are also included. For type I ELMy H-mode plasma, the ELM frequency is around 50–80 Hz and the induced losses are typically of the order of 10% of the total plasma stored energy. For N seeded and detached discharges, the ELMy frequency is more than 200 Hz and the stored energy losses are around 2% of the total plasma stored energy. Measurements from 1.5 ms before the ELM onset to at least 4 ms after the ELM crash are excluded for the type I ELMy H-mode plasma. Due to the much smaller ELM amplitudes (≈ 5 times

lower) at very high ELM frequencies, no time points were excluded for the N seeded and detached discharges.

3. Transport study in the near SOL region

3.1. Parallel transport in the near SOL region

Previous study [2] shows that the simple relation of $\lambda_{T_{e,u}} = \frac{7}{2} \lambda_{q_{||e}}$, derived from application of the two-point model with Spitzer–Harm parallel thermal transport, is found to relate $\lambda_{T_{e,u}}$ and $\lambda_{q_{||e}}$ for ASDEX Upgrade H-mode attached plasma well, which means the SOL is in the conduction-limited regime. Since whether the parallel transport is dominated by Spitzer–Harm classical conduction is very important for the rest of study in this paper, a test whether the upstream and downstream measurements for the extended dataset can be described by the relation $\lambda_{T_{e,u}} = \frac{7}{2} \lambda_{q_{||e,u}}$ is performed in section.

A previous empirical study [21, 22], based on downstream IR measurements, found that $\lambda_{q_{||e}}$ in ASDEX Upgrade discharges could be well described by the following scalings:

$$\lambda_{q_{||e}} = (0.78 \pm 0.69) B_T^{-0.63 \pm 1.05} q_{\text{cyl}}^{1.14 \pm 0.81} \times P_{\text{sol}}^{-0.05 \pm 0.31} \text{ for } H\text{-mode attached plasma}$$

and

$$\lambda_{q_{||e}} = (1.45 \pm 0.13) B_T^{-0.78} q_{\text{cyl}}^{1.07 \pm 0.07} \times P_{\text{sol}}^{-0.14 \pm 0.05} \text{ for } L\text{-mode attached plasma.}$$

Here, $\lambda_{q_{||e}}$ is measured in mm; B_T is measured in Tesla; q_{cyl} is the cylindrical safety factor; and P_{sol} is measured in MW. For the L-mode study [22], since all discharges were conducted at the same B_T , the dependence of $\lambda_{q_{||e}}$ on B_T was assumed to be the same as for the H-mode scaling based on the resulting multi-machine databases [21].

To test the consistency between the IR measurements and the TS measurements, the above empirical scalings are compared. Figure 2 compares the upstream T_e decay length, $\lambda_{T_{e,u}}$ from TS measurements, with the prediction of the scalings based IR measurements for type I ELMy H-mode, nitrogen seeded H-mode and L-mode discharges under attached divertor condition. For L-mode discharges, since the dependence on B_T is not derived from experimental data and the majority of the dataset is comprised of discharges with $B_T \approx 2.5$ T, a constant value of $B_T^{-0.78} = 2.5^{-0.78}$ is used in the scaling. As shown in figure 1, the value of $\lambda_{T_{e,u}}/\lambda_{q_{||e}}$ lies in the range 3.5 ± 1 for the H-mode attached plasma and in the range 3.5 ± 0.8 for L-mode attached regime. The spread is consistent with the measurement uncertainties. Thus, across the wide set of plasma parameters and regimes in the dataset, the results are consistent with $\lambda_{T_{e,u}} = \frac{7}{2} \lambda_{q_{||e}}$. A flux limited correction to the heat flux, as described in [23, 24], would be small for the plasmas of this dataset. In figure 2(a), the nitrogen seeded discharges seem to be more scattered. Due to the very high ELM frequencies and small ELM amplitudes, no effort was taken to cut out ELM affected time points from

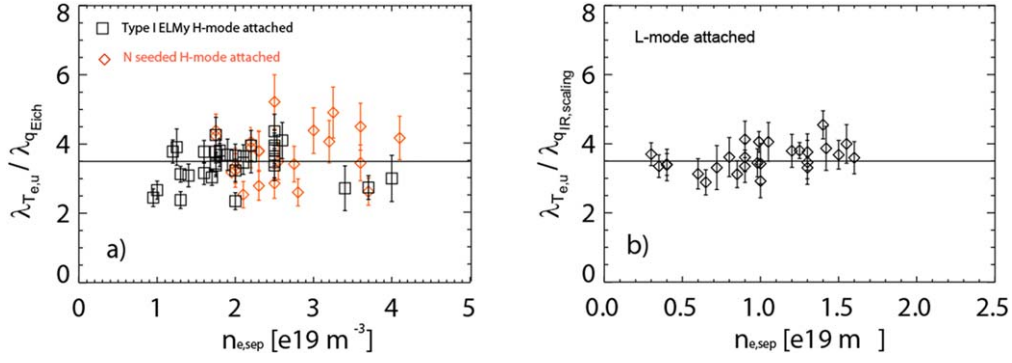


Figure 2. Comparison of upstream T_e decay length, $\lambda_{T_{e,u}}$, from TS measurements with the prediction of the scalings derived from IR measurements for AUG (a) type I ELMy H-mode and N seeded H-mode discharges under attached divertor condition; and (b) L-mode attached discharges.

the TS data for nitrogen seeded discharges. The cause of the scattering is most likely the influence of ELMs on the measured, $\lambda_{T_{e,u}}$. As shown in [25], the scattering is observed to be larger at higher J_p . Thus, it has been shown that the upstream near SOL for the entire attached H-mode and L-mode dataset used in this paper is consistent with the SOL being in the Spitzer–Harm classical conduction limit. The fact that this applies to attached N seeded AUG H-mode too, is a new result. The outer divertor radiation varies between about 20% and 50% of the separatrix power, with the N seeded scenarios at the upper end of this interval. With no or very low seeding, the divertor radiation is produced mainly by B, C and O; with strong N seeding, N radiation dominates.

3.2. Perpendicular transport in the near SOL region

The perpendicular thermal diffusivity, χ_{\perp} , in the near SOL can be derived from the experimental data using power balance. In the near SOL, thermal transport is assumed to be dominated by parallel and perpendicular heat flux. In steady state, the parallel flow of the heat poloidally, from upstream to the divertor target, balances the perpendicular flow of the heat radially. This can be described by the formula:

$$P_{SOL} = q_{\parallel} A_{\parallel} = q_{\perp} A_{\perp}. \quad (1)$$

Here, the parallel heat flux, q_{\parallel} , is given by $q_{\parallel} = -\kappa_{0e} T_e^{5/2} \nabla_{\parallel} T_e = -\kappa_{0e} T_e^{5/2} \frac{T_{e,u}}{\pi q R}$ and $A_{\parallel} = 4\pi R \lambda_{q_{\parallel}} B_{\theta} / B_T$ is the surface area for the parallel flux. The cross-field perpendicular heat flux, q_{\perp} , can be expressed as $q_{\perp} = -n_{e,u} \chi_{\perp} \nabla_{\perp} T_e = -n_{e,u} \chi_{\perp} \frac{T_{e,u}}{\lambda_{T_{e,u}}}$, where, χ_{\perp} is the perpendicular thermal diffusivity and the surface area for the perpendicular flux is $A_{\perp} = 2\pi a \cdot 2\pi R$. Equation (1) then gives

$$\chi_{\perp} \propto n_{e,u}^{-1} \lambda_{T_{e,u}}^2 q_{95}^{-2} T_{e,u}^{5/2} R^{-2}. \quad (2)$$

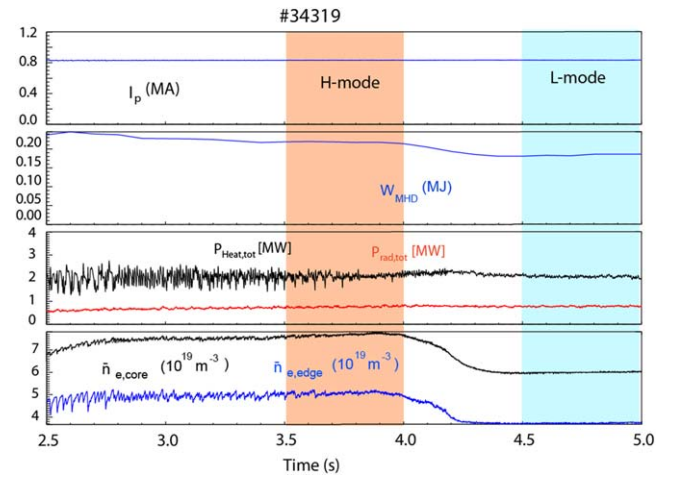


Figure 3. Time traces of AUG discharge #34319: plasma current (I_p), plasma stored energy (W_{MHD}), total heating power and total radiation ($P_{Heat,tot}$ and $P_{rad,tot}$), line integrated edge and core electron density ($\bar{n}_{e,edge}$ and $\bar{n}_{e,core}$).

This expression relates the perpendicular thermal diffusivity to the measured electron temperature decay length. The formula is now used to determine the change in perpendicular transport for a H- to L-mode back transition. Figure 3 shows the characteristic time traces of an H-/L-mode transition discharge. After the onset of the H-mode, the total heating power remains constant and the electron density is gradually increased. As the density increases, the minimum required power to sustain H-mode also increases. At $t \approx 4$ s, the heating power starts to be lower than the power threshold and the H–L back transition occurs. To compare the SOL profiles for the two phases, half second steady plasma just before the transition (as indicated in red) and half second steady state after transition (in blue) are shown in figure 4. For the H-mode phase, $\lambda_{T_{e,u}} \approx 11.4$ mm. For the L-mode phase,

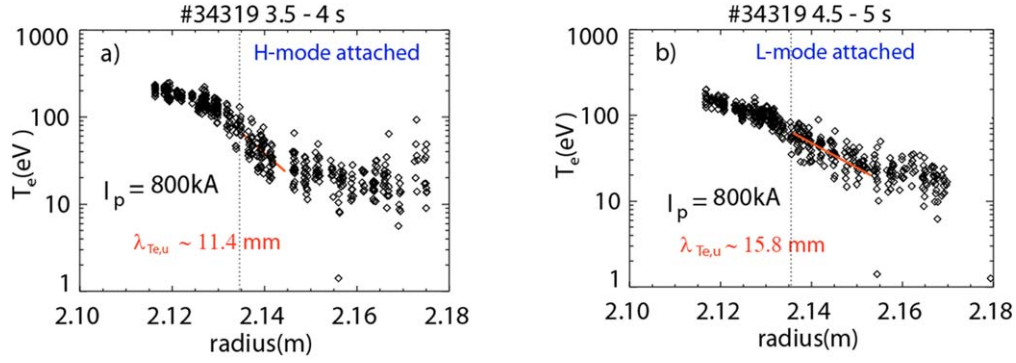


Figure 4. Electron temperature, T_e , profiles, for the AUG discharge of figure 2, in the (a) H-mode regime, and (b) L-mode regime.

$\lambda_{T_{e,u}} \approx 15.8$ mm, giving $\lambda_{T_{e,u}}^L / \lambda_{T_{e,u}}^H \approx 1.4$. In the conduction-limited regime, the separatrix temperature can be estimated by

$$T_{e,u} \approx \left(\frac{7 (P_{\text{SOL}} / A_{q_1}) L}{2 \kappa_{0e}} \right)^{2/7}. \quad (3)$$

Here, for the estimation of P_{SOL} , there is little information about how the power entering the SOL divides between the electron and ion channels, so it is simply assumed that $P_{\text{SOL}}^e \approx P_{\text{SOL}} \approx P_{\text{tot}} - P_{\text{rad,main}}$. Although P_{SOL} remains constant during the transition, the parallel flux surface increases due to the broadening of SOL, with $T_{e,u}^L / T_{e,u}^H \approx 0.9$. The electron density decreases after the back transition, with $n_{e,u}^L / n_{e,u}^H \approx 0.8$. So, the impact of the change of the local parameters in equation (2) during the back transition is largely compensated by each other, with the relevant term in equation (2), $\sqrt{n_{e,u} T_{e,u}^{-5/2}}$, changing by less than 5%. Instead, the broadening of the temperature profile is mainly due to the increase of the perpendicular transport. From equation (2), the estimated relative increase in the electron thermal diffusivity is $\chi_{\perp}^L / \chi_{\perp}^H \approx 2$.

This example shows that the ‘bifurcation’ in the core plasma between H- and L-mode regimes also exists in the perpendicular transport in the near SOL region, and that the hypothesis of one single scaling for both H- and L-mode, posited in [4], is incorrect.

Assuming different coefficients for different regimes, a log-linear regression over the combined H-mode and L-mode dataset, with respect to q_{95} and P_{SOL} , gives the following best fit scaling:

$$\lambda_{T_{e,u}} = C_{H,L} q_{95}^{0.82 \pm 0.12} P_{\text{sol}}^{-0.14 \pm 0.06} \times (C_H = 2.6; C_L = 3.8, C_L / C_H \approx 1.4). \quad (4)$$

This regression has a fit quality of $R^2 = 0.95$. As data is derived from a single tokamak, AUG, the geometric radius of the plasma, R , does not vary greatly within the present database, so size dependence is not considered in the fit. Similarly, as the majority of dataset for both L-mode and H-mode is comprised of discharges with $B_T \approx 2.5$ T, B_T is also excluded from the scaling. As shown in figure 5, the dataset is well represented by this scaling with no obvious systematic deviations. Applying equation (3) to the scaling in equation (4) gives the alternative form $\lambda_{T_{e,u}} \propto C_{H,L} q_{95}^{0.91} T_{e,u}^{-0.46}$. This expression is consistent with the

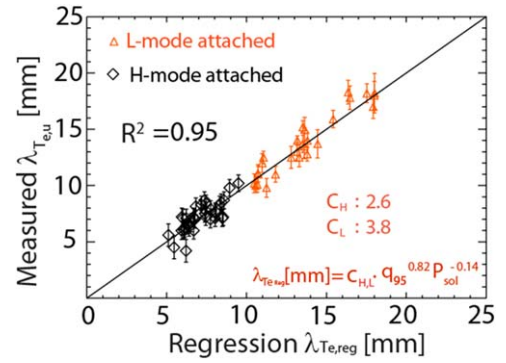


Figure 5. Upstream electron temperature decay length, $\lambda_{T_{e,u}}$, measured from TS system against the scaling with different coefficients for AUG H and L-mode plasma, $\lambda_{T_{e,u}} = C_{H,L} q_{95}^{0.82 \pm 0.12} P_{\text{sol}}^{-0.14 \pm 0.06}$ ($C_H = 2.6$; $C_L = 3.8$, $C_L / C_H \approx 1.4$).

H–L back transition already discussed. Combining equation (2) with the expression $\lambda_{T_{e,u}} \propto C_{H,L} q_{95} T_{e,u}^{-1/2}$ gives $\chi_{\perp} \propto C_{H,L}^x n_e^{-1} T_e^{3/2}$ (C_H^x for H-mode plasma, C_L^x for L-mode plasma, $C_L^x / C_H^x \approx 2$). In this case, the cross-field transport has same parametric dependences in H- and L-mode plasma, but with same local parameters, the perpendicular transport for L-mode is about twice that of the H-mode regime.

3.3. Study with plasmas under detached divertor condition

In a previous study [2], the near SOL electron temperature profile is observed to broaden under completely detached divertor condition. The broadening of $\lambda_{T_{e,u}}$ is accompanied by the flattening of density profile, as shown in figure 6. Figure 6(a) shows a typical reference H-mode discharge, #30975, under attached divertor conditions with $\lambda_{T_{e,u}} \approx 6.5 \pm 0.8$ mm and $\lambda_{n_{e,u}} \approx 9 \pm 1$ mm. In discharge #31647, with the same plasma current (1 MA), the density was increased, using Kr seeding, to achieve the detached divertor condition. As can be seen in figure 6(b), for this detached plasma, both temperature and density profiles are broader than the reference, with $\lambda_{T_{e,u}} \approx 12.5 \pm 1.2$ mm and $\lambda_{n_{e,u}} \approx 18 \pm 1.5$ mm. The feature of density profile flattening in the SOL region has been observed in earlier studies of L-mode plasmas, where the phenomenon has been called the L-mode HDT [8–10]. A more recent study [11] shows that

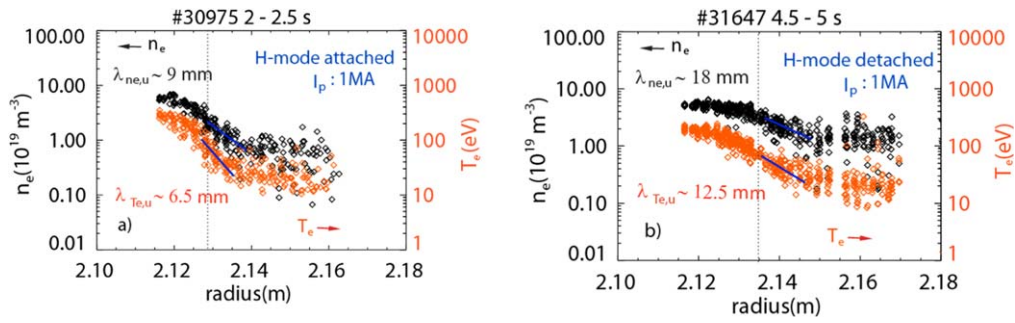


Figure 6. Electron temperature, T_e , and density, n_e , against major radius at the midplane for plasma in the (a) H-mode attached regime, #30975; and (b) H-mode detached regime with Kr seeding, #31647.

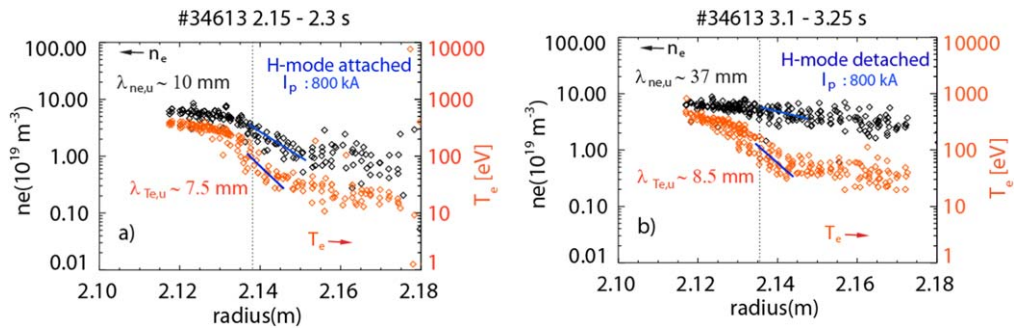


Figure 7. Electron temperature, T_e , and density, n_e , against major radius at the midplane for the AUG N seeded discharge #34613 in the (a) H-mode attached regime; and (b) H-mode detached regime.

filaments appear as a result of the interchange instability which enhances perpendicular particle transport, as high collisionality in the SOL may trigger a regime transition leading to strongly enhanced perpendicular particle fluxes. The observation of broadening of both temperature and density profiles under detached divertor condition suggests that the filaments may also enhance the perpendicular heat transport. This will be investigated here.

Figure 7 presents the transition of a H-mode plasma from attached to detached divertor conditions by nitrogen seeding without the cryo-pump. As the line average density increases from $\bar{n}_e = 7.5 \times 10^{19} \text{ m}^{-3}$ to $1.0 \times 10^{20} \text{ m}^{-3}$, the density profile in the SOL changes, flattening its gradient: the two-zone structure changes into one ‘shoulder’ with $\lambda_{n_{e,u}} \approx 37 \text{ mm}$, figure 7(b). However, the electron temperature gradient length, $\lambda_{T_{e,u}} \approx 8.5 \pm 1.1 \text{ mm}$, is almost identical to that of the attached plasma, $\lambda_{T_{e,u}} \approx 7.5 \pm 1.2 \text{ mm}$. This shows that, for this discharge, the filaments which enhance the perpendicular particle transport have little influence in the heat transport channel.

The principle difference between the discharges of figures 6(b) and 7(b), that may drive the different SOL thermal transport, is the different seeded ion species. As reported in early studies [26–29], nitrogen seeding has generally been shown to improve global plasma energy confinement in metal-walled machines. This motivates the study of the relationship between global plasma energy confinement and the change in SOL transport between attached and detached plasmas. In figure 8, a group of discharges with same I_p , and B_T under attached and detached conditions is chosen to study the correlation between $\lambda_{T_{e,u}}$ and H_{98} , the global plasma

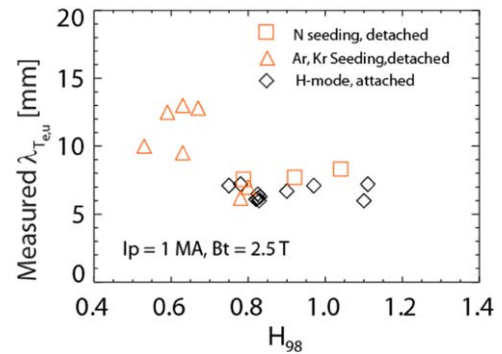


Figure 8. SOL temperature decay length, $\lambda_{T_{e,u}}$, against global energy confinement time normalized to the IPB98(y, 2) scaling, H_{98} , for AUG H-mode attached and detached plasmas.

energy confinement time normalized to the empirical IPB98 (y, 2) multi-machine ELMy H-mode scaling [30]. Under detached conditions, the discharges with broadened profiles also have much lower normalized confinement, while those with unchanged profiles have similar normalized confinement to attached plasma.

Based on the near SOL transport study in sections 3.1 and 3.2, the SOL electron temperature decay length for the present AUG dataset has been shown to be well described by $\lambda_{T_{e,u}} \propto q_{95} T_{e,u}^{-1/2}$. For the same q_{95} , the temperature profile would expect to be broader with lower separatrix temperature. To study its impact on detached plasmas, it is assumed that, under detached divertor condition, the parallel heat transport is still dominated by collisional conduction, hence, equation (3) can still be used to estimate $T_{e,u}$. Figure 9 shows

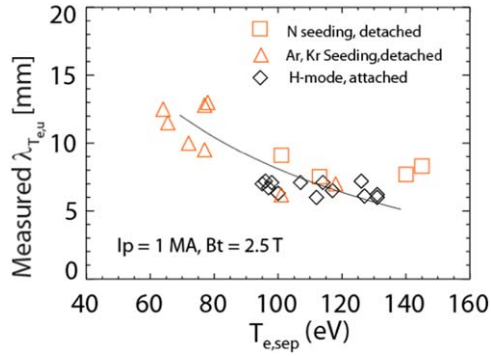


Figure 9. SOL temperature decay length, $\lambda_{T_{e,u}}$, against separatrix temperature, $T_{e,sep}$, for AUG H-mode attached and detached plasmas. The gray line describes $\lambda_{T_{e,u}} \propto T_{e,u}^{-1/2}$.

$\lambda_{T_{e,u}}$ against $T_{e,u}$ for the same discharges shown in figure 8. Under detached conditions, the discharges with broader profiles also have much lower $T_{e,u}$ due to much lower P_{sol} , while those with unchanged profiles have similar temperature at the separatrix with attached plasma. In this figure, the gray line describes the relation $\lambda_{T_{e,u}} \propto T_{e,u}^{-1/2}$. Thus, the change in $\lambda_{T_{e,u}}$ between the detached and attached ELMy H-mode plasmas is consistent with a dependence on global confinement or separatrix temperature.

4. Relating to the properties in the confined region

As discussed in section 1, several studies have identified a general trend for higher pressure and temperature gradients in the pedestal region of the plasma core to be associated with higher temperature gradients, and hence lower $\lambda_{T_{e,u}}$, in the near SOL region [2, 14–17]. These include comparisons between H-mode and L-mode plasmas, studies of attached H-modes with different global plasma parameters, and comparisons between attached and fully detached plasmas. Taken together, these observations suggest that the pedestal region plays an important role in setting the decay length in the near SOL. This section presents a study of two examples that break the trend and, hence, show that it is not causal.

The first case is a comparison between nitrogen seeded ELMy H-mode and unseeded type I ELMy H-mode plasmas. Significant increases in the achievable pedestal top pressure are observed with N seeding, in particular at high heating powers, and are correlated with inward shifted density profiles and a reduction of the high field side high density region (the HFSHD) [28, 29]. Figure 10, shows two discharges with the same plasma current, $I_p = 1$ MA and toroidal field $B_T = 2.5$ T. Discharge 30974 is a typical type I ELMy H-mode with $\bar{n}_e = 7.8 \times 10^{19} \text{ m}^{-3}$ and $P_{tot} = 3$ MW. Discharge #32959 is a N seeded ELMy H-mode discharge under attached condition with $\bar{n}_e = 8.5 \times 10^{19} \text{ m}^{-3}$ and $P_{tot} = 13$ MW. Regarding the power entering the SOL, $P_{sol} = 1.7$ MW for Discharge #30974 and $P_{sol} = 5$ MW. As can be seen from figure 10(a), the pedestal top pressure for N seeded discharge is more than twice that of the standard H-mode reference. However, the SOL T_e decay length, $\lambda_{T_{e,u}}$, is

almost the same, 6–6.5 mm, and, indeed, within the measurement uncertainties, about 10% in both cases. This result contradicts the proposition that the pedestal region plays an important role in setting the decay length in the near SOL. Figure 11 shows the correlation between $\lambda_{T_{e,u}}$ and the pedestal top electron pressure, $p_{e,ped}$, for the full database of AUG type I ELMy H-modes and N seeded ELMy H-modes. Although there is a clear negative correlation between the T_e SOL decay length and the pedestal top pressure for type I ELMy H-mode plasmas, such a trend is broken when N seeded discharges are considered. This further supports the proposition that the $\lambda_{T_{e,u}} - p_{e,ped}$ correlation is a consequence of both parameters depending on other parameters, such as plasma current [2], rather than a direct dependence of one on another.

The second case that will be studied here is the transition to the so-called improved energy confinement regime (I-mode). In I-mode plasma, an increase of the edge temperatures with a concomitant steepening of the edge gradients builds a temperature pedestal similar to that of the H-mode. In I-mode, intermittent turbulence events have been observed in the confinement region, which are linked to the weakly coherent mode [31, 32]. These events cause radial transport across the separatrix and are later observed in the divertor [31]. The events increase the heat flux onto the divertor, but do not seem to change SOL width. In contrast to the H-mode, the I-mode edge density profile is much broader and, indeed, very similar to that of the L-mode. Thus, a comparison of L-mode and I-mode plasma provides a good way to investigate the impact of temperature pedestal gradient on SOL decay width, while for relatively fixed pedestal density gradient.

A good example of an AUG I-mode discharge, #30865, is described detailed in [32]. In this discharge, the ECRH heating power was increased every 500 ms, while, the density remained almost constant. The discharge moves from an L-mode, to a weak I-mode, and then to an I-mode phase with the core pedestal and SOL temperature and density profiles illustrated in figure 12. The discharge begins in L-mode until, around $t \approx 3.18$ s, the electron temperature and pressure gradients and the global confinement increase slightly at constant heating power. This spontaneous confinement transition is considered as a transition from an L-mode to a weak I-mode. With additional heating power at $t = 3.5$ s, H_{98} increases above 0.6 and a clear I-mode develops: the electron temperature gradients strongly increase, while the density gradient remains almost unchanged. The SOL temperature profiles for the three phases are illustrated in figure 13. The L-mode phase, figure 13(a), has a wide SOL, with $\lambda_{T_e} \approx 11$ mm. In the weak I-mode regime, figure 13(b), the near SOL is much narrower, $\lambda_{T_e} \approx 7$ mm. The SOL T_e profile in the I-mode regime, figure 13(c), is almost same as the one in the weak I-mode regime, with $\lambda_{T_e} \approx 6.6$ mm, despite the large increase of pedestal gradient. This shows that, in the transition from weak I-mode to I-mode, the generally observed correlation between the T_e SOL decay length and the pedestal top pressure is also broken and so it is non-causal.

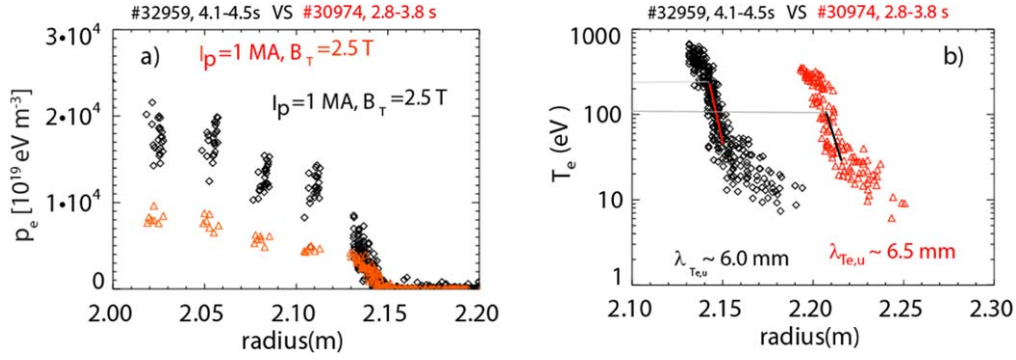


Figure 10. (a) Electron pressure, p_e , against major radius at the midplane for AUG N seeded discharge #32959 (in black) and standard H-mode discharge #30974 (in red), with identical plasma currents and toroidal fields. (b) Electron temperature, T_e , against major radius at the midplane for the same discharges and time windows.

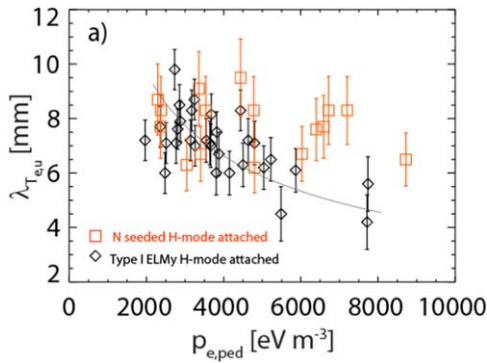


Figure 11. SOL T_e decay length, $\lambda_{T_{e,u}}$, against pedestal top pressure, $p_{e,ped}$, for the AUG type I ELMy H-mode dataset (black diamonds) and N seeded discharges (red squares.) The gray line describe the relations $\lambda_{T_e} \propto P_{e,ped}^{-0.6}$.

5. Summary and discussion

A database of unseeded type I ELMy H-modes, N seeded H-modes, and unseeded L-mode discharges has been constructed from ASDEX Upgrade discharges with TS data suitable for the analysis of the upstream SOL electron profiles and the correlation with the properties in the confined region. Even though the database now extends over a wide density range ($n_{e,sep} = (1 - 5) \times 10^{19} \text{ m}^{-3}$), the simple relation, $\lambda_{q_{||e}} = \frac{2}{7} \lambda_{T_{e,u}}$, relates the upstream measured electron temperature width, $\lambda_{T_{e,u}}$, with the scaling for the power decay length, deduced from downstream IR measurements, well. This means that the analyzed ASDEX Upgrade dataset is in the conduction-limited regime, i.e. the parallel transport in the near SOL is dominated by Spitzer–Harm conduction. The fact that this applies to attached N seeded AUG H-mode too, is a new result. Based on the equations from the Spitzer–Harm conduction and power balance, a simple relation can be deduced to derive the perpendicular heat transport coefficient, χ_{\perp} from the measured parameters.

Previous studies based on downstream IR camera and the midplane profiles from TS system show that the SOL decay widths have similar parametric dependences in H- and L-mode plasma. Whilst there was evidence a separate scaling, with different pre-multiplying coefficients, for H-mode and

L-mode, it had been shown that the available datasets could also be well described by a single scaling for H and L-mode plasma. In this paper, study of a H- to L-mode back transition obtained by increasing the electron density shows that a ‘bifurcation’ does exist in the perpendicular transport between the H- and L-mode. Even with fixed global plasma parameters and the same power entering the SOL, the profile in the near SOL region is broader after the transition to L-mode, with $\lambda_{T_{e,u}}^L / \lambda_{T_{e,u}}^H \approx 1.4$. Analysis shows that the broadening is mainly due to sudden increase of perpendicular transport. From the relation, $\lambda_{T_{e,u}} \propto q_{95} R \sqrt{n_{e,u} T_{e,u}^{-5/2} \chi_{\perp}}$, it is estimated that $\chi_{\perp}^L / \chi_{\perp}^H \approx 2$. Based on the observed bifurcation between H- and L-mode plasma in the SOL region and assuming similar parametric dependences with different coefficient for each regime, the scaling $\lambda_{T_{e,u}} = C_{H,L} q_{95}^{0.82 \pm 0.12} P_{sol}^{-0.14 \pm 0.06}$ ($C_H = 2.6$; $C_L = 3.8$; $C_L / C_H \approx 1.4$) is found to fit H- and L-mode plasmas. For the same plasma parameters, $\lambda_{T_{e,u}}$ in the near SOL for the L-mode regime is roughly 1.4 times broader than that for H-mode regime. By using power balance in the SOL, this scaling can be used to derived the following expression for the SOL perpendicular thermal diffusivity $\chi_{\perp} \propto C_{H,L}^{\chi} n_e^{-1} T_e^{3/2}$ (C_H^{χ} for H-mode plasma, C_L^{χ} for L-mode plasma, $C_L / C_H \approx 2$). The cross-field transport has the same parametric dependences in H- and L-mode plasma, but, for the same local plasma parameters, the perpendicular transport for L-mode is about twice that for the H-mode regime.

For detached plasmas, the SOL upstream electron profile is found to be broader than an equivalent attached plasma under certain conditions. This was assumed to be correlated with the formation of the ‘shoulder’ in the density profile in the SOL region when the collisionality reaches a critical value, referred to as the HDT. Although, there are cases where both temperature and density profiles become broader above a certain density, consistent with this model, there are also examples where $\lambda_{T_{e,u}}$ remains almost constant at densities above that where the density profile becomes significantly flatter. Hence, the onset of the broadening of temperature profile is not consistent with the onset of ‘shoulder’ formation. By comparing $\lambda_{T_{e,u}}$ with global energy confinement, it is found that the discharges with broadened profiles also have degraded confinement, while those with unchanged profiles have similar confinement to attached plasma. By assuming

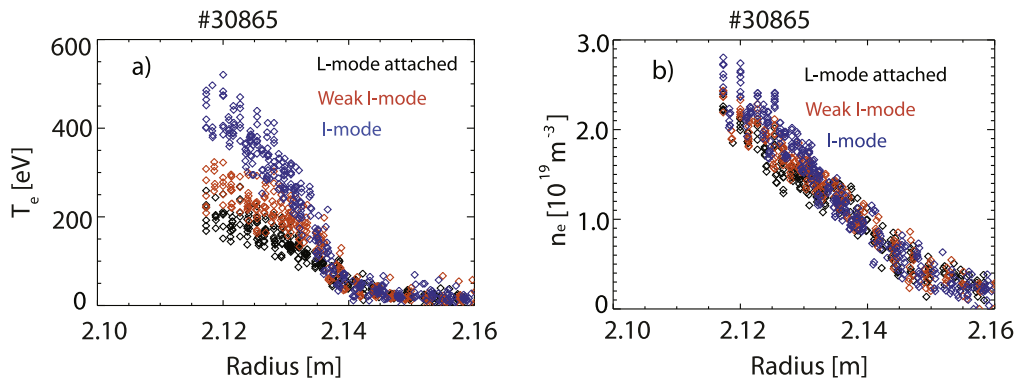


Figure 12. (a) Electron temperature, T_e , and (b) electron density, n_e , against major radius at the midplane across the core pedestal and near SOL region of the AUG I-mode discharge #30865.

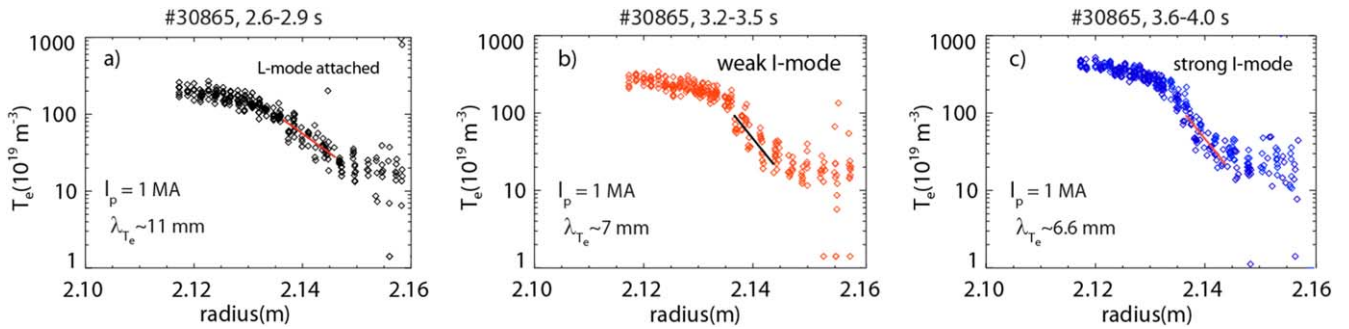


Figure 13. Electron temperature, T_e , against major radius at the midplane for the AUG discharge #30865 in L-mode regime (a), weak I-mode regime (b), and I-mode regime (c).

the parallel heat transport in the near SOL region is still dominated by conduction, upstream temperature can be estimated by the same equation used in the attached regime. By this method, the widening of the SOL is found to coincide with the dropping of upstream temperature.

For the H–L back transition, a bifurcation exists between H and L-mode plasma, the change of profiles in the near SOL is similar to that in the pedestal region: the profile is steeper in the H-mode regime and becomes flatter after the transition into L-mode regime. Under detached conditions, the discharges with the broadest profiles are associated with those that undergo degradation of core confinement, while those with unchanged profiles tend to have confinement similar to that of equivalent attached plasma. In addition, for type I ELM H-mode discharges, a general trend of smaller pedestal pressure gradients and pedestal pressure top is associated with a broader $\lambda_{T_{e,u}}$ in the near SOL region, as presented in [2]. These observations seem to support the proposition that the pedestal region plays an important role in setting the decay length in the near SOL, consistent with previous results [14–17]. However, when the data is restricted to single plasma current, the same tendency is not observed. To test this hypothesis, two examples, where the general trend appears to be broken were identified and studied.

The first case related to the significant increases in the achievable pedestal top pressure which are observed with N seeding, in particular at high heating powers. A nitrogen seeded discharge with such a recipe was used to test the influence of pedestal region on the near SOL region. It is

found that, even when the pedestal top pressure increases by more than a factor of two, the profile in the near SOL remains almost the same. The second case, was the transition from L-mode to I-mode plasma which provides a good way to investigate the impact of varying temperature pedestal gradient on SOL decay width, under conditions where the plasma density profiles vary relatively little. By gradually increasing the heating power, an AUG discharge was made to transit from L-mode to weak I-mode and then I-mode. A steep temperature gradient built up gradually: slightly steepening in the weak I-mode regimes as the confinement increases; the gradient then strongly increases and the confinement increases by 60% when a clear I-mode develops. Interestingly, the SOL becomes significantly narrower when a weak I-mode is achieved, while, from the weak I-mode to the I-mode, $\lambda_{T_{e,u}}$ is almost constant within measurement uncertainties, despite a strongly increasing of pedestal gradient. Taken together, the two cases discussed here both break the generally observed correlation between the T_e SOL decay length and the pedestal top pressure. Hence, the relationship is non-causal and must instead be due to similar dependences on other plasma parameters, such as plasma current. Importantly for next step devices, this negates the proposition of section 1, that higher confinement is desired in the core plasma can only be achieved at the expense of a larger heat flux in the divertor. The two may be varied independently and plasma with higher global energy confinement and lower heat flux in the divertor may be achievable.

If the generally observed strong correlation between the pedestal and SOL regions is not direct, and so causal, how is it explained? In particular, how is the simultaneous change of profiles in both regions during the H–L back transition explained? It is well accepted that the suppression of turbulence by the shear flow in the plasma edge is the reason for the transition to the H-mode regime. From the example of the H–L back transition in this paper, it is clear that the SOL perpendicular transport undergoes a bifurcation between the H- and L-mode. This suggests that, in the H-mode regime, the shear flow also suppresses the perpendicular transport across the separatrix and, thus, affects the profiles in the near SOL. For the detached divertor condition, the correlation between $\lambda_{T_{e,u}}$ and H factor also seems to imply that core confinement influences the near SOL. This could be explained by the cooling of plasma due to impurity radiation. A previous study [33] of high radiated power H-mode plasma shows that plasma with high Z impurities and associated degraded confinement also tend to have a much lower temperature just inside the separatrix. In this case, the reduction of parallel heat transport due to the lower temperature will broaden λ_{Te} for the detached plasma caused by high Z impurity seeding. Since the same trend is broken when the plasma current is fixed, the general trend of smaller pedestal pressure gradients/top being associated with a broader $\lambda_{T_{e,u}}$ in the near SOL region can be explained by the co-dependence on plasma global parameters, like plasma current.

Acknowledgments

This work has been carried out within the framework of the EUROfusion Consortium and has received funding from the European Union's Horizon 2020 research and innovation programme under grant agreement number 633053. The views and opinions expressed herein do not necessarily reflect those of the European Commission.

ORCID iDs

H J Sun  <https://orcid.org/0000-0003-0880-0013>

T Eich  <https://orcid.org/0000-0003-3065-8420>

A Kallenbach  <https://orcid.org/0000-0003-0538-2493>

References

- [1] Stangeby P C 2000 *The Plasma Boundary of Magnetic Fusion Devices* (Bristol: Institute of Physics Publishing)
- [2] Sun H J et al 2015 *Plasma Phys. Control. Fusion* **57** 125001
- [3] Faitsch M et al 2015 *Plasma Phys. Control. Fusion* **57** 075005
- [4] Sun H J et al 2017 *Plasma Phys. Control. Fusion* **59** 105010
- [5] Counsell G et al 1999 *J. Nucl. Mater.* **266–269** 91
- [6] Connor J et al 1999 *Nucl. Fusion* **39** 169
- [7] Leonard A et al 2016 *Int. Conf. on Plasma Surface Interactions in Controlled Fusion Devices (Rome)*
- [8] LaBombard B et al 2001 *Phys. Plasma* **8** 2107
- [9] Asakura N et al 1997 *J. Nucl. Mater.* **241** 559
- [10] McCormick K et al 1992 *J. Nucl. Mater.* **196–198** 264–70
- [11] Carralero D et al 2015 *Phys. Rev. Lett.* **2** 21500
- [12] Carralero D et al 2018 *Nucl. Fusion* **58** 096015
- [13] Fedorczak N et al 2017 *Nucl. Mater. Energy* **12** 838
- [14] LaBombard B et al 2011 *Phys. Plasma* **18** 056104
- [15] Loarte A et al 1999 *J. Nucl. Mater.* **266–269** 587
- [16] Schweinzer J et al 1997 *Proc. 24th EPS Conf. Cont. Fusion Plasma Phys.* vol 21A p 1449
- [17] Neuhauser J et al 2002 *Plasma Phys. Control. Fusion* **44** 855
- [18] Kallenbach A et al 2003 *Nucl. Fusion* **43** 573
- [19] Kurzan B et al 2011 *Rev. Sci. Instrum.* **82** 103501
- [20] Kallenbach A et al 2018 *Plasma Phys. Control. Fusion* **60** 045006
- [21] Eich T et al 2011 *Phys. Rev. Lett.* **107** 215001
- [22] Sieglin B et al 2016 *Plasma Phys. Control. Fusion* **58** 055015
- [23] Stangeby P et al 2015 *Nucl. Fusion* **55** 093014
- [24] Leonard A et al 2017 *Nucl. Fusion* **57** 086033
- [25] Kallenbach A et al 2018 *Plasma Phys. Control. Fusion* **60** 045006
- [26] Reinke M et al 2011 *J. Nucl. Mater.* **415** S340
- [27] Beurskens M et al 2013 *Plasma Phys. Control. Fusion* **55** 024043
- [28] Dunne M G et al 2017 *Plasma Phys. Control. Fusion* **59** 014017
- [29] Dunne M G et al 2017 *Plasma Phys. Control. Fusion* **59** 025010
- [30] ITER Physics Expert Group on Confinement 1999 ITER physics basis *Nucl. Fusion* **39** 2391
- [31] Happel T et al 2017 *Plasma Phys. Control. Fusion* **59** 014004
- [32] Manz P et al 2015 *Nucl. Fusion* **55** 083004
- [33] Loarte A et al 2011 *Phys. Plasma* **18** 056105